# Differentiation of germinal center B cells into plasma cells is initiated by high-affinity antigen and completed by Tfh cells

Nike J. Kräutler,[1]* Dan Suan,[1]* Danyal Butt,[1] Katherine Bourne,[1] Jana R. Hermes,[1] Tyani D. Chan,[1,3] Christopher Sundling,[1] Warren Kaplan,[2,3] Peter Schofield,[1] Jennifer Jackson,[1] Antony Basten,[1,3] Daniel Christ,[1,3] and Robert Brink[1,3]

[1]Immunology Division and [2]Kinghorn Centre for Clinical Genomics, Garvan Institute of Medical Research, Darlinghurst NSW 2010, Australia
[3]St. Vincent's Clinical School, University of New South Wales, Darlinghurst NSW 2010, Australia

**Plasma cells (PCs) derived from germinal centers (GCs) secrete the high-affinity antibodies required for long-term serological immunity. Nevertheless, the process whereby GC B cells differentiate into PCs is uncharacterized, and the mechanism underlying the selective PC differentiation of only high-affinity GC B cells remains unknown. In this study, we show that differentiation into PCs is induced among a discrete subset of high-affinity B cells residing within the light zone of the GC. Initiation of differentiation required signals delivered upon engagement with intact antigen. Signals delivered by T follicular helper cells were not required to initiate differentiation but were essential to complete the differentiation process and drive migration of maturing PCs through the dark zone and out of the GC. This bipartite or two-signal mechanism has likely evolved to both sustain protective immunity and avoid autoantibody production.**

The Journal of Experimental Medicine

## INTRODUCTION

Germinal centers (GCs) are transient structures that form around the follicular dendritic cell (FDC) networks located within secondary lymphoid organs 4–7 d after challenge with foreign T cell–dependent antigens (Gatto and Brink, 2010; Victora and Nussenzweig, 2012). Antigen-specific B cells recruited into GCs undergo somatic hypermutation (SHM) of the Ig variable region genes that encode the binding specificity of the clonal B cell receptor (BCR). Clones acquiring increased affinity for antigen via SHM are preferentially retained within the GC in a process known as positive selection (Berek et al., 1991; Jacob et al., 1991). In addition, differentiation of GC B cells into antibody-secreting plasma cells (PCs) is restricted to those with high affinity for antigen (Smith et al., 2000; Phan et al., 2006). Together, these processes ensure that the GC output is made up of the most effective antibodies possible, thus providing the basis for long-term serological immunity after infection and vaccination (Plotkin et al., 2008).

GC B cells consist of spatially and phenotypically distinct light-zone (LZ) and dark-zone (DZ) populations with $CXCR4^{lo}$ $CD86^{hi}$ and $CXCR4^{hi}$ $CD86^{lo}$ cell surface phenotypes, respectively (Victora et al., 2010; Bannard et al., 2013). The signals that sustain GC B cell responses are localized within the LZ in the form of (a) intact antigen displayed on the surface of FDCs and (b) T follicular helper cells (Tfh cells) that bind processed antigenic peptides presented with class II MHC molecules on the B cell surface (Gatto and Brink, 2010; Victora and Nussenzweig, 2012). LZ B cells transit to the DZ where they undergo cell division and SHM before returning to the LZ. Preferential activation of high-affinity GC B cells in the LZ is widely accepted to mediate positive selection. However, PCs appear to exit from the DZ of the GC (Meyer-Hermann et al., 2012), and it remains unclear where and how PC differentiation is initiated within GCs. Conclusions drawn from mathematical modeling (Meyer-Hermann et al., 2006), two-photon microscopy (Allen et al., 2007), and loading of GC B cells with extrinsic peptide (Victora et al., 2010) have led to the suggestion that high-affinity GC B cells receive enhanced Tfh cell help. However, definitive identification of the stimulus that determines selective differentiation of high-affinity GC B cells into PCs awaits detailed characterization of the differentiation process within GCs and the impact of specific abrogation of signals delivered by direct engagement of intact antigen on FDCs versus those provided by Tfh cell help.

## RESULTS AND DISCUSSION

To facilitate such a study, we developed a high-resolution in vivo model in which the phenotype and fate of high- and low-affinity GC B cells are clearly identifiable. CD45.1-marked B cells from $SW_{HEL}$ mice, expressing the anti–hen egg lysozyme (HEL) specificity of the HyHEL10 mAb (Phan et al.,

*N.J. Kräutler and D. Suan contributed equally to this paper.

Correspondence to Robert Brink: r.brink@garvan.org.au

N.J. Kräutler's present address is ETH Zürich, Institute of Microbiology, 8093 Zürich, Switzerland.

Abbreviations used: BCR, B cell receptor; DZ, dark zone; FDC, follicular dendritic cell; GC, germinal center; GSEA, gene set enrichment analysis; HEL, hen egg lysozyme; LZ, light zone; PC, plasma cell; SHM, somatic hypermutation; SRBC, sheep RBC; Tfh cell, T follicular helper cell.



The Rockefeller University Press $30.00
J. Exp. Med. 2017 Vol. 214 No. 5 1259–1267
https://doi.org/10.1084/jem.20161533

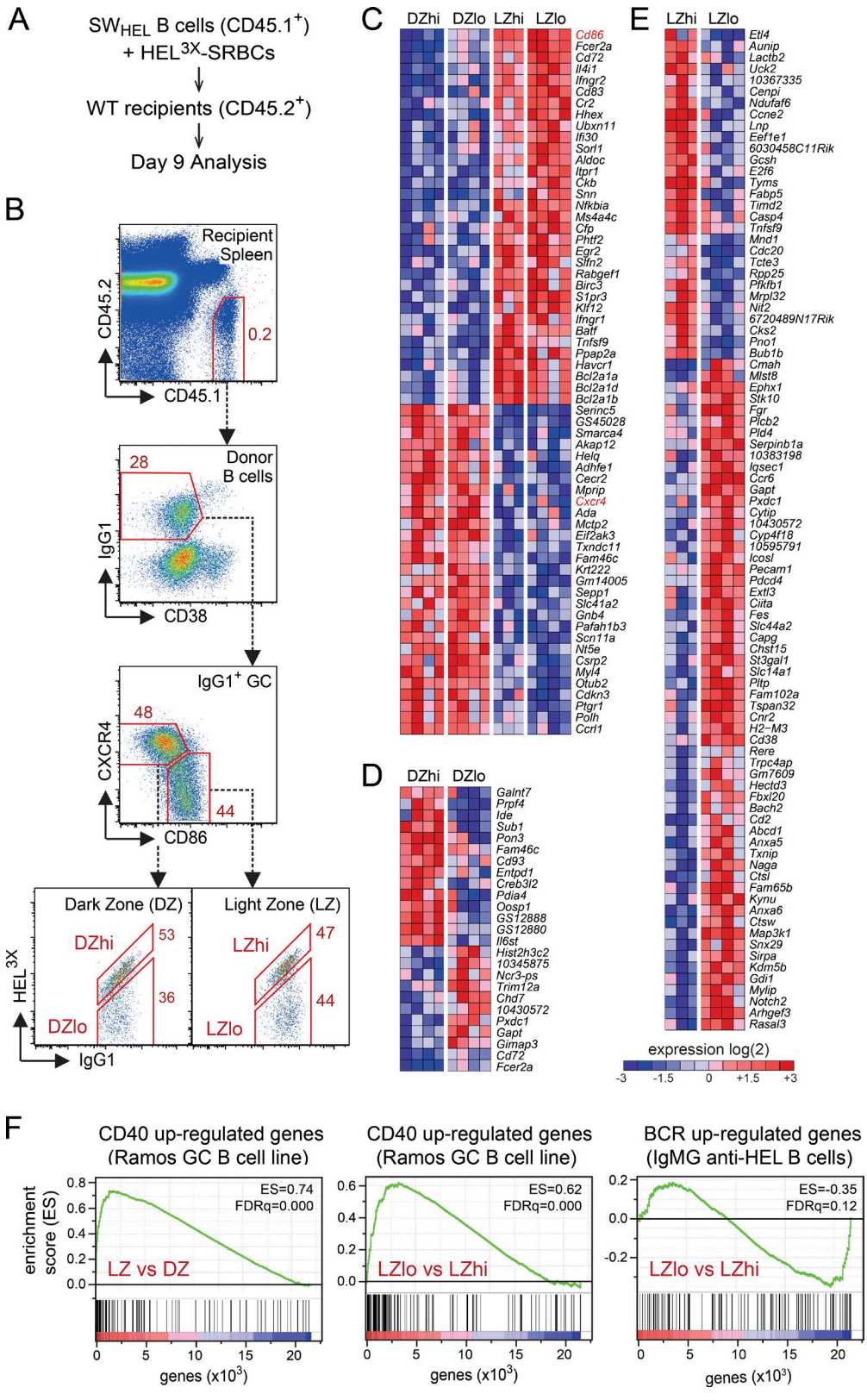


Figure 1. **Identification of high- and low-affinity LZ and DZ $SW_{HEL}$ GC B cells and their affinity-dependent gene expression signatures.** (A) General experimental strategy. (B) Flow cytometric gating used to sort and characterize donor-derived $SW_{HEL}$ GC B cells. $IgG1^+$ GC B cells are resolved into high- and low-affinity DZ and LZ populations (DZhi, DZlo, LZhi, and LZlo). (C) Heat map showing genes differentially expressed between DZ and LZ GC B

2003), were transferred into wild-type (CD45.2$^+$) recipient mice and challenged with the low-affinity ($K_a \sim 10^7$ M$^{-1}$) HEL$^{3X}$ protein coupled to sheep RBCs (SRBCs; HEL$^{3X}$-SRBCs; Fig. 1 A; Paus et al., 2006; Chan et al., 2012). Donor SW$_{HEL}$ B cells form GCs on days 4–5 of the response (Chan et al., 2009) and undergo affinity-based selection to HEL$^{3X}$. By day 9, ∼50% of IgG1-switched LZ and DZ B cells possess high affinity for HEL$^{3X}$ (i.e., LZhi/DZhi GC B cells) as defined by flow cytometric staining with limiting HEL$^{3X}$ (Fig. 1 B). High-affinity SW$_{HEL}$ GC B cells carry the Y53D Ig heavy chain substitution (Fig. S1; Phan et al., 2006), which conveys an ∼100-fold increase in HEL$^{3X}$-binding affinity (Chan et al., 2012).

Using gene expression microarray analysis, we confirmed that HEL$^{3X}$-specific LZ and DZ GC B cells differentially express a core set of 62 genes regardless of antigen affinity (Fig. 1 C) and that this gene expression signature corresponds closely to that previously identified in anti-NP GC responses (Fig. S2 A; Victora et al., 2010). However, upon further analysis, we found additional sets of genes displaying affinity-dependent expression, particularly within the LZ compartment (Fig. 1, D and E). Gene set enrichment analysis (GSEA) confirmed previous findings (Victora et al., 2010) that LZ rather than DZ GC B cells possess a gene expression signature that most closely mirrors that of a GC B cell line (Ramos) after CD40 ligand (CD40L) stimulation (Fig. 1 F, left; Basso et al., 2004). Interestingly, this signature was stronger in LZlo compared with LZhi cells (Fig. 1 F, middle), suggesting that LZhi cells may receive signals other than those derived from Tfh cells. A gene expression signature derived from antigen-stimulated B cells expressing a BCR with an IgG1 cytoplasmic tail (Horikawa et al., 2007) showed a slightly stronger similarity to LZhi versus LZlo GC B cells (Fig. 1 F, right). Overall, however, it was not possible to make strong conclusions about the signals delivered to LZhi versus LZlo GC B cells on the basis of gene expression profiling alone.

We next set out to (a) characterize the process of PC differentiation within the GC and (b) identify the impacts on this process of specific abrogation of antigen engagement versus Tfh cell help. We found that DZ B cells displayed a more prominent PC gene signature (Mori et al., 2008) than LZ B cells (Fig. S2 B), with DZhi cells in particular expressing canonical PC genes (e.g., *Prdm1/Blimp1*, *Sdc1*, *Cd93*, *Igj*, and *Xbp1*; Fig. 2 A) and exhibiting a strong PC gene expression signature relative to DZlo cells (Fig. 2 B). Nevertheless, a PC gene signature was also evident in LZhi versus LZlo cells (Fig. 2 C), and analysis of responses from SW$_{HEL}$ B cells carrying the *Blimp1$^{gfp}$* reporter gene (Kallies et al., 2004) confirmed that PC-lineage cells (*Blimp1*-GFP$^+$) are present within both the DZhi and LZhi compartments (Fig. 2 D and Fig. S2 C). Based on established PC biology (Kallies et al., 2004), we hypothesized that the GC cells with lowest *Blimp1*-GFP reporter and highest BCR (IgG1) expression were those most recently committed to PC differentiation. This was supported by the fact that *Blimp1*-GFP$^{lo}$ IgG1$^{hi}$ cells expressed higher levels of B220 and CD45 than *Blimp1*-GFP$^{hi}$ IgG1$^{lo}$ PC-lineage cells (Fig. 2 E; Jensen et al., 1989; Lalor et al., 1992). Significantly, we found that *Blimp1*-GFP$^+$ cells in the LZ almost exclusively possess an early PC-lineage phenotype (*Blimp1*-GFP$^{lo}$ IgG1$^{hi}$; Fig. 2 F). Therefore, our data indicated that PC differentiation is initiated by signals delivered to LZhi GC B cells, with subsequent transition to a late PC phenotype (*Blimp1*-GFP$^{hi}$ IgG1$^{lo}$) occurring after migration into the DZ. This is consistent with a previous report that presumptive PC-lineage cells expressing high levels of the *Blimp1*-inducing transcription factor IRF4 (Sciammas et al., 2006) are present in the LZ of human tonsillar GC (Falini et al., 2000) and that the LZhi compartment defined in the present study displays the highest levels of *Irf4* mRNA expression in the GC (Fig. 2 A).

To interrogate the specific roles of Tfh cell help versus antigen engagement in PC differentiation, we again challenged transferred SW$_{HEL}$.*Blimp1$^{gfp/+}$* B cells with HEL$^{3X}$-SRBCs. On day 6 of the response (after GC formation), recipients were injected with mAbs that block (anti-CD40L) or deplete (anti-CD4) Tfh cell help, and the effect on GC responses was assessed 3 d later (day 9; Fig. 3, A and B). To block BCR access to FDC-bound antigen (HEL$^{3X}$), recipients were injected with HyHEL10*, a soluble IgG1 homologue of the SW$_{HEL}$ BCR carrying three heavy chain mutations (S31R, Y53D, and Y58F) that confer very high affinity ($K_a > 10^{-10}$ M$^{-1}$; Chan et al., 2012) for HEL$^{3X}$. To exclude possible FcγR-mediated effects in this case, control recipients were injected with HyHEL9, an IgG1 mAb that binds HEL and HEL$^{3X}$ with very high affinity ($K_a > 10^{-10}$ M$^{-1}$) but does not compete with HyHEL10 (Fig. 3 A; Smith-Gill et al., 1984).

Treatment with either HyHEL10* anti-CD4 or CD40L for 3 d led to similar (40–60%) reductions in the overall size of the GC response, with the DZ compartment most impacted in each case (Fig. S3 A). However, only antigen blockade with HyHEL10* abolished PC differentiation, removing both early (*Blimp1*-GFP$^{lo}$ IgG1$^{hi}$) and late (*Blimp1*-GFP$^{hi}$ IgG1$^{lo}$) PC-lineage cells (Fig. 3, C and D). The fact that both anti–Tfh cell treatments reduced GC size without preventing PC differentiation indicated that the abrogation of PC

cells regardless of BCR antigen affinity. Genes encoding markers used to define the DZ and LZ subsets (*Cd86* and *Cxcr4*) are indicated in red. The fold-change cutoff was set to ≥1.5984 (= fold-change up-regulation of *Cxcr4* in DZ vs. LZ) with P ≤ 0.0005. (D and E) Heat maps showing genes differentially expressed according to BCR antigen affinity within either the DZ (D) or LZ (E). (F) GSEA of relative gene expression in total LZ versus total DZ GC B cells (left) or LZlo versus LZhi GC B cells (middle) against the gene set identified as up-regulated after CD40L stimulation of the human GC B cell line Ramos (Basso et al., 2004) and LZlo versus LZhi GC B cells against genes up-regulated by antigen (HEL) stimulation of B cells expressing an IgM BCR with an IgG1 cytoplasmic tail (Horikawa et al., 2007). FDRq, false discovery rate. Gene expression data represent four independent experiments of 25 mice per experiment.

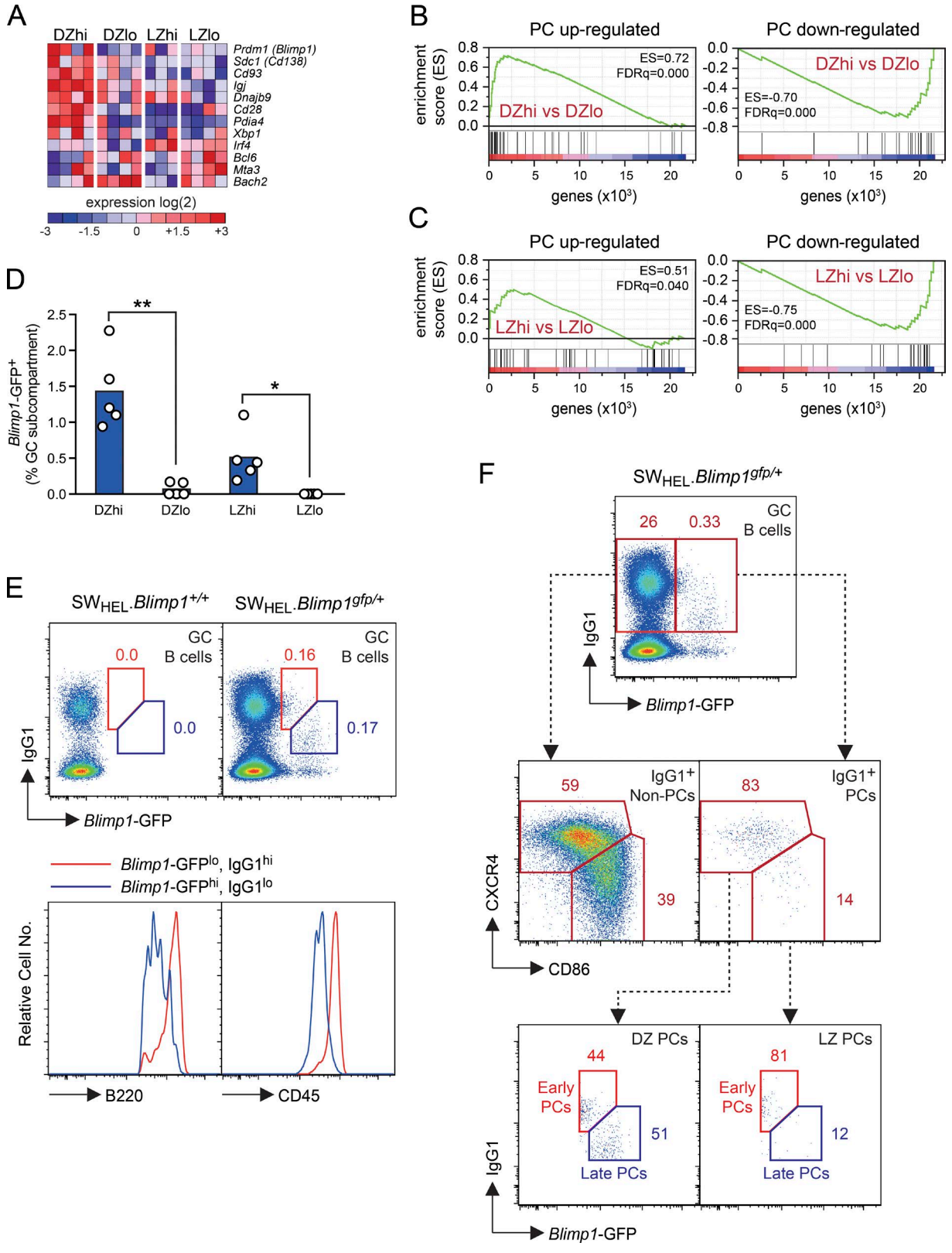


Figure 2. **Identification of early and late PC-lineage cells in the GC and enrichment of early PCs in the LZ.** (A) Heat map of selected genes known to be up-regulated (top eight) or down-regulated (bottom three) in PCs, indicating a strong PC gene expression signature in the DZhi compartment. (B and C) GSEA of differential gene expression according to antigen affinity within the DZ (B) and LZ (C) compartments, against gene sets either up-regulated (left)

differentiation by HyHEL10* cannot be attributed to impaired antigen presentation and reduced Tfh cell help. Instead, HyHEL10* must act by preventing delivery of signals normally imparted to LZhi GC B cells directly upon antigen engagement. The specific impact of antigen blockade on the induction of PC differentiation was also evident after 2 d of HyHEL10* treatment (from days 7 to 9), which selectively depleted early PC-lineage cells (Fig. 3, E and F) including all LZ phenotype cells (not depicted). Analysis of the IgG1$^-$ (predominantly IgG2b$^+$) PC-lineage cells in the GC showed similar results (not depicted), indicating that the triggering of the PC differentiation pathway by antigen engagement is a mechanism that is likely to apply generally to IgG-switched GC responses.

Although the overall numbers of PC-lineage cells were largely unchanged by abrogation of Tfh cell help, anti-CD4 (but not anti-CD40L) treatment had a pronounced qualitative impact. Thus, in direct contrast to antigen blockade, Tfh cell depletion resulted in the relative enrichment of early PC-lineage cells (Fig. 3, C and D). Accordingly, anti-CD4 (but not anti-CD40L) treatment also increased the fraction of PC-lineage cells that exhibited an LZ phenotype (Fig. 4, A and B). To determine whether this shift in the phenotype of PC-lineage cells was associated with physical retention in the LZ, immunofluorescence histology was undertaken. PC-lineage cells were identifiable by their strong cytoplasmic expression of IgG1 and localized primarily within the DZ of control GCs before appearing to exit through the base of the DZ (Fig. 4 C and Fig. S3 B; Meyer-Hermann et al., 2012). As has been described previously (Angelin-Duclos et al., 2000; Meyer-Hermann et al., 2012), many PC-lineage cells (30–40% by our enumeration) are found in small clusters in or just outside the GC, suggesting that ongoing cell division may occur during early PC differentiation. LZ PC-lineage cells were in natural proximity to LZ-resident FDCs (Fig. 4 C), raising the possibility that they may access antigen via the immune complexes displayed on the FDC surface. Strikingly, LZ PC-lineage cells were greatly enriched in GCs from mice treated with anti-CD4 (Fig. 4 C). LZ retention of PC-lineage cells was not seen upon treatment with anti-CD40L (Fig. S3 C), confirming that Tfh cell–derived signals other than CD40L are required to drive the LZ egress and phenotypic maturation of LZhi GC B cells that have been previously licensed to initiate PC differentiation upon direct engagement of antigen.

The exquisite selectivity of PC differentiation for high-affinity GC cells (Phan et al., 2006) means that its underlying mechanism must be tightly linked to antigen affinity. This condition is clearly satisfied by our finding that signals delivered upon antigen engagement are responsible for the initiation of PC differentiation among LZhi GC B cells. Although it remains unclear whether LZhi cells present more peptide antigen than LZlo cells, our gene microarray data raise the question of whether LZhi cells do preferentially receive Tfh cell help (Victora et al., 2010; Shinnakasu et al., 2016). A determining role for Tfh cells in driving PC differentiation had been proposed based on the finding that GC B cells undergo DZ migration and PC differentiation en masse when they are loaded with exogenous peptide recognized by resident Tfh cells (Victora et al., 2010). Our observations do indeed support the conclusion that Tfh cell help promotes DZ migration of committed PC-lineage cells, interestingly via signals other than CD40L. However, because depletion of Tfh cell help did not impact upon the initiation of PC differentiation in our study, we argue that boosting of Tfh cell help with exogenous peptide provides a supraphysiological stimulus to GC B cells that can drive PC differentiation regardless of BCR affinity, much like B cells stimulated with excess CD40L and cytokines in vitro (Hodgkin et al., 1994). Thus, although Tfh cell help is clearly required to progress PC differentiation and migration within the GC, it is signals delivered directly upon BCR engagement of intact antigen, most likely from the surface of FDCs, that initiate this process under physiological conditions. Therefore, our findings recall the bipartite two-signal paradigm of immune activation originally proposed by Bretscher and Cohn (1970) to prevent activation of self-reactive lymphocytes. Applied to the dynamic BCR repertoire of somatically mutating GC B cells, the need for a discriminating signal 1 (engagement of high-affinity antigen) to be supplemented with signal 2 (cognate Tfh cell help) provides a mechanism not only for selective production of high-affinity antiforeign antibodies, but also of preventing production of high-affinity autoantibodies that can arise because of chance SHM events (Brink, 2014).

The specific nature of the stimulus that initiates PC differentiation after engagement of FDC-bound antigen remains unclear. Although there are conflicting data regarding the ability of the BCRs of GC B cells to deliver intracellular signals (Khalil et al., 2012; Nowosad et al., 2016), many ligands associated with FDCs can engage GC BCRs and may act with or without BCR signaling to initiate PC differentiation. These include complement fragments (e.g., C3d), adhesion molecules (ICAM-1/VCAM-1), IL-6, B cell–activating factor, and C4BP (El Shikh et al., 2010; Goodnow et al., 2010). An intriguing question is whether signals delivered directly upon antigen

or down-regulated (right) in PCs (Mori et al., 2008). FDRq, false discovery rate. (D) Proportion of cells within each of the four GC subcompartments detected as *Blimp1*-GFP$^+$ on day 9 of the $SW_{HEL}$.*Blimp1*$^{gfp/+}$ response to HEL$^{3X}$-SRBCs. (E, top) Day 9 GC B cells derived from $SW_{HEL}$.*Blimp1*$^{+/+}$ and $SW_{HEL}$.*Blimp1*$^{gfp/+}$ donor B cells resolving *Blimp1*-GFP$^{lo}$, IgG1$^{hi}$, and *Blimp1*-GFP$^{hi}$ IgG1$^{lo}$ subpopulations. (Bottom) Histogram overlays showing higher B220 and CD45 staining on the *Blimp1*-GFP$^{lo}$ IgG1$^{hi}$ population. (F) Flow cytometric analysis of the LZ and DZ phenotypes of *Blimp1*-GFP$^+$ IgG1$^+$ GC B cells. Data from are representative of five independent experiments of five mice per group. Flow cytometry plots are concatenated data from five recipient mice. P-values were calculated using a paired Student's *t* test. *, $0.01 \leq P < 0.05$; **, $0.001 \leq P < 0.01$.

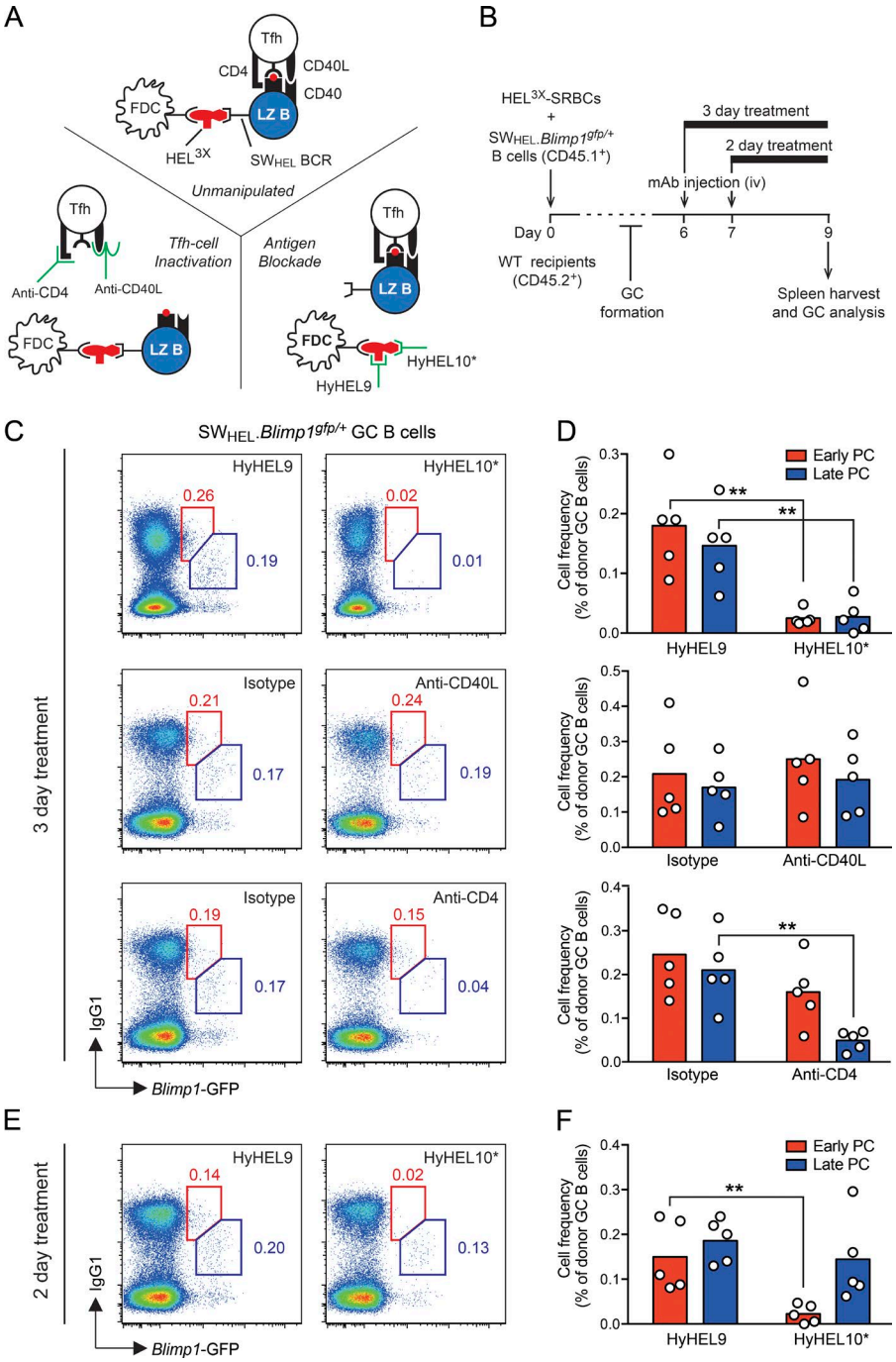


Figure 3. **Blocking antigen access, but not Tfh cell help, prevents initiation of PC differentiation in the GC.** (A) Schematic of antigen engagement and reception of cognate CD4$^+$ Tfh cell help by $SW_{HEL}$ B cells in unmanipulated GCs (top), plus the mAb-based approaches used to specifically block Tfh cell help (bottom left) or block engagement of intact antigen by the $SW_{HEL}$ BCR (bottom right). Both HyHEL10* and HyHEL9 bind to $HEL^{3X}$, but only HyHEL10* blocks access to the antigen by the $SW_{HEL}$ BCR. (B) Experimental design for mAb-blocking experiments. $SW_{HEL}$.*Blimp1*$^{gfp/+}$ B cells were permitted to form GCs in response to $HEL^{3X}$-SRBCs and recipients and then given a single injection of mAbs 2 or 3 d before spleen harvest and analysis on day 9. (C and D) Impact of 3 d of mAb treatment on IgG1$^+$ PC-lineage cells in GCs derived from $SW_{HEL}$.*Blimp1*$^{gfp/+}$ donor B cells. Representative flow cytometry profiles are shown (C), as well as enumeration of early (*Blimp1*-GFP$^{lo}$ IgG1$^{hi}$) and late (*Blimp1*-GFP$^{hi}$ IgG1$^{lo}$) PC-lineage populations in individual recipients (D). (E and F) Impact of 2 d of HyHEL10* treatment analyzed as for C and D. Data from each mAb treatment are representative of two to four independent experiments of five mice per group. Flow cytometry plots are concatenated data from five recipient mice. P-values were calculated using an unpaired Student's *t* test. **, $0.001 \leq P < 0.01$.

engagement as opposed to enhanced antigen presentation may also be the primary driver of positive selection in the GC. The iterative nature of positive selection as opposed to the linear progression of PC differentiation makes this a more difficult issue to resolve. However, the clear implication of our findings is that either (a) antigen engagement acts as the master regulator of both positive selection and PC differentiation within the GC or (b) these two key processes rely on distinct selective mechanisms.

## MATERIALS AND METHODS

### Mice, adoptive transfers, and in vivo antibody treatments

$SW_{HEL}$ mice (Phan et al., 2003) were maintained on a congenic CD45.1 (*Ptprc*$^{a/a}$) C57BL/6 background. To facilitate tracking of PC differentiation, $SW_{HEL}$ mice were interbred with *Blimp1*$^{gfp/+}$ mice (Kallies et al., 2004). For adoptive transfers, 6–10-wk-old wild-type C57BL/6 recipient mice (Australian BioResources) received $3 \times 10^4$ HEL-binding $SW_{HEL}$ B cells intravenously in combination with $2 \times 10^8$

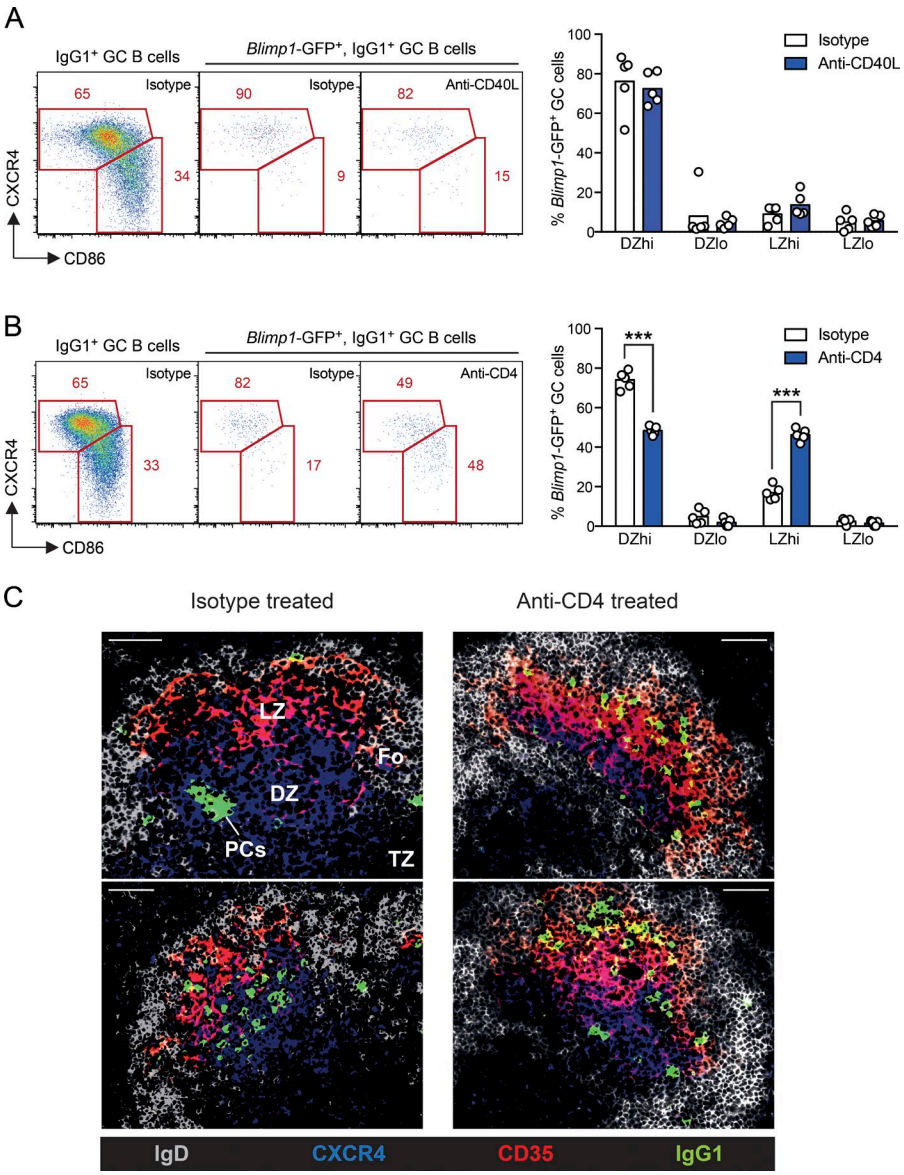


Figure 4. **PC-lineage cells are enriched in the LZ after depletion of CD4$^+$ Tfh cells and colocalize with FDCs.** (A and B) GC responses were established from $SW_{HEL}$.*Blimp1*$^{gfp/+}$ B cells and subjected to 3-d treatment with either anti-CD40L (A) or anti-CD4 (B) as outlined in Fig. 3. (Left) Representative flow cytometry profiles indicate the impact of mAb treatments on the LZ and DZ phenotypes of IgG1$^+$ PC-lineage cells (*Blimp1*-GFP$^+$). (Right) The proportions of IgG1$^+$ PC-lineage cells that fell within the DZhi, DZlo, LZhi, and LZlo compartments in individual recipients were also enumerated. (C) Immunofluorescence histology of spleens from recipient mice 9 d after transfer of $SW_{HEL}$ B cells plus $HEL^{3X}$-SRBCs and 3 d after injection of isotype control or anti-CD4 mAb. The B cell follicle (Fo) is marked by IgD (white), the LZ by CD35 (FDCs; red), and the DZ by CXCR4 (blue). The unstained T cell zone (TZ) is also indicated. IgG1$^+$ PC-lineage cells are identifiable by bright (cytoplasmic) staining (green). Frequencies of IgG1$^+$ PC-lineage cells identified within the LZ (containing CD35$^+$ FDCs) by immunofluorescence analysis were 7% (5/66) in isotype-treated and 69% (76/110) in anti-CD4–treated mice (enumerated over 17 and 16 individual GCs, respectively). Bars, 50 µm. Data are representative of two to four independent experiments of five mice per group (A and B) or are representative of four independent experiments of five mice per group (C). P-values were calculated using an unpaired Student's *t* test. ***, P < 0.001.

$HEL^{3X}$-conjugated SRBCs (Paus et al., 2006). To block interaction of GC B cells with Tfh cells or native antigen, mice were treated with 200 µg anti-CD4 (GK1.5; rat IgG2b; Bio X Cell), 200 µg anti-CD40L (MR-1; hamster IgG; University of California, San Francisco [UCSF] Monoclonal Antibody Core), or 50 µg HyHEL10* (HyHEL10 carrying Y53D/S31R/Y58 mutations; mouse IgG1; produced in house) at the indicated time points. Control groups received equal amounts of the respective isotype control antibodies. Animal studies were approved and conducted in compliance within the guidelines set down by the Garvan/St.Vincent's Animal Ethics Committee.

### HEL proteins and HyHEL antibodies

Recombinant $HEL^{3X}$ was produced in yeast (*Pichia pastoris*) and purified from culture supernatants as previously described (Paus et al., 2006). HyHEL10* IgG1 mAb was expressed in HEK293 cells and purified as previously described (Butt et al., 2015), and HyHEL9 was supplied by the UCSF Monoclonal Antibody Core.

### Flow cytometry

Recipient splenocytes were prepared and stained for cell surface $HEL^{3X}$ and IgG1 as previously described (Chan et al., 2012) and subsequently incubated with the additional directly conjugated antibodies and streptavidin reagents. Donor-derived ($SW_{HEL}$) GC B cells were identified as CD45.1$^+$, CD45.2$^-$, B220$^+$, and CD38$^{lo}$ (Fig. 1 B). Flow cytometric data were acquired on an LSRII SORP flow cytometer (BD), and data were analyzed by FlowJo software (Tree Star). For sort purification of single (SHM analysis) or bulk GC B cells, samples were isolated using a FACSAria III flow cytometer (BD).

### SHM analysis

Single LZhi, LZlo, DZhi, and DZlo IgG1$^+$ $SW_{HEL}$ GC B cells (see gates in Fig. 1 B) were sorted into 96-well plates, and the variable region exon of the $SW_{HEL}$ immunoglobulin heavy chain variable region exon (HyHEL10) was PCR amplified and sequenced as previously described (Paus et al., 2006).

### mRNA microarray and computational data analysis

$SW_{HEL}$ B cell subpopulations (minimum 16,800 cells) were gated as outlined in Fig. 1 B and sorted directly into TRIzol (Invitrogen), and RNA extraction was performed according to the manufacturer's instructions. To improve recovery, RNA was precipitated with GlycoBlue (Thermo Fisher Scientific). RNA quality and quantity was determined using a Bioanalyzer 2100 (Agilent Technologies). RNA samples were reverse transcribed, amplified, labeled, and fragmented using Ovation Pico WTA, WT Ovation Exon Module, and Encore Biotin Module (NuGen) and hybridized with a whole-transcript gene array on a Mouse Gene 1.0 ST array chip by the Ramaciotti Centre for Genomics (University of New South Wales). One of four LZhi samples did not pass the quality control data assessment of the microarray (Console) and was therefore excluded from the analysis. Computational analysis of gene expression was performed on GenePattern (data normalization, determination of differential gene expression by LimmaGP, and GSEA preranked by fold-change; Broad Institute). For generation of heat maps, transcripts were excluded if they failed to reach a minimal mean expression of log2(x) ≥4. Cutoffs (fold-change and p-values) are indicated in the relevant figures. Genes displayed in heat maps were hierarchically clustered using Pearson correlation.

### Immunofluorescence histology

Splenic cryosections were prepared and stained as previously described (Chan et al., 2009) using the antibodies and fluorescent reagents. Slides were imaged on an upright microscope (DM5500; Leica Biosystems), and images were analyzed using Photoshop CS5 (version 12.1; Adobe). Strong staining was observed for PC-lineage cells expressing high levels of cytoplasmic IgG1 in addition to weak cell surface staining for IgG1$^+$ GC B cells. For clarity, images of IgG1$^+$ cells presented in this study show only the brightly staining PC-lineage cells.

### Statistical analysis

Statistical analyses were undertaken using a paired or unpaired two-tailed Student's *t* test in Prism (GraphPad Software). Significant p-values are indicated in figures for the following ranges: *, $0.01 \leq P < 0.05$; **, $0.001 \leq P < 0.01$; ***, $P < 0.001$. In all summary figures, each data point represents an individual mouse, and bars represent the mean. In bar graphs, error bars represent standard error of the mean.

### Accession no.

Gene expression microarray data were deposited to the Gene Expression Omnibus under accession no. GSE94638.

### Online supplemental material

Fig. S1 shows the SHM analysis in the four GC compartments on day 9 of the response of $SW_{HEL}$ B cells to $HEL^{3X}$-SRBCs. Fig. S2 shows GSEA analyses of LZ and DZ gene expression signatures and flow cytometric detection of *Blimp1*-GFP$^+$ PC-lineage cells in the four GC compartments. Fig. S3 shows the effects of antibody treatments on GC size and composition as well as additional immunofluorescence histology analysis of IgG1$^+$ PC-lineage cells within GC structures.

## ACKNOWLEDGMENTS

We thank the staff of Australian BioResources for animal husbandry, the staff of the Garvan Institute Flow Cytometry Facility for cell sorting, the Ramaciotti Centre for Genomics for microarray analysis, and C. Goodnow and T.G. Phan for discussions and comments on the manuscript.

N.J. Kräutler was supported by the Swiss National Science Foundation (grant PMPDP3_175146), C. Sundling by the Swedish Research Council (grant 2013-7333), D. Butt by an Australian Postgraduate Award, and D. Suan, T.D. Chan, D. Christ, and R. Brink by the National Health and Medical Research Council (NHMRC). This work was funded by NHMRC Program Grant 1016953.

The authors declare no competing financial interests.

Author contributions: N.J. Kräutler and D. Suan designed and performed experiments, interpreted the results, and prepared the manuscript. D. Butt, K. Bourne, and J.R. Hermes performed several experiments. T.D. Chan and C. Sundling helped with experimental design. W. Kaplan helped with microarray analyses. P. Schofield and J. Jackson prepared key reagents. A. Basten and D. Christ helped with experimental design and research supervision. R. Brink designed experiments, supervised research, and wrote the manuscript.

**Submitted: 13 September 2016**

**Revised: 15 November 2016**

**Accepted: 15 February 2017**

## REFERENCES

Allen, C.D., T. Okada, H.L. Tang, and J.G. Cyster. 2007. Imaging of germinal center selection events during affinity maturation. *Science.* 315:528–531. http://dx.doi.org/10.1126/science.1136736

Angelin-Duclos, C., G. Cattoretti, K.I. Lin, and K. Calame. 2000. Commitment of B lymphocytes to a plasma cell fate is associated with Blimp-1 expression in vivo. *J. Immunol.* 165:5462–5471. http://dx.doi.org/10.4049/jimmunol.165.10.5462

Bannard, O., R.M. Horton, C.D.C. Allen, J. An, T. Nagasawa, and J.G. Cyster. 2013. Germinal center centroblasts transition to a centrocyte phenotype according to a timed program and depend on the dark zone for effective selection. *Immunity.* 39:912–924. http://dx.doi.org/10.1016/j.immuni.2013.08.038

Basso, K., U. Klein, H. Niu, G.A. Stolovitzky, Y. Tu, A. Califano, G. Cattoretti, and R. Dalla-Favera. 2004. Tracking CD40 signaling during germinal center development. *Blood.* 104:4088–4096. http://dx.doi.org/10.1182/blood-2003-12-4291

Berek, C., A. Berger, and M. Apel. 1991. Maturation of the immune response in germinal centers. *Cell.* 67:1121–1129. http://dx.doi.org/10.1016/0092-8674(91)90289-B

Bretscher, P., and M. Cohn. 1970. A theory of self-nonself discrimination. *Science.* 169:1042–1049. http://dx.doi.org/10.1126/science.169.3950.1042

Brink, R. 2014. The imperfect control of self-reactive germinal center B cells. *Curr. Opin. Immunol.* 28:97–101. http://dx.doi.org/10.1016/j.coi.2014.03.001

Butt, D., T.D. Chan, K. Bourne, J.R. Hermes, A. Nguyen, A. Statham, L.A. O'Reilly, A. Strasser, S. Price, P. Schofield, et al. 2015. FAS inactivation releases unconventional germinal center B cells that escape antigen control and drive IgE and autoantibody production. *Immunity.* 42:890–902. http://dx.doi.org/10.1016/j.immuni.2015.04.010

Chan, T.D., D. Gatto, K. Wood, T. Camidge, A. Basten, and R. Brink. 2009. Antigen affinity controls rapid T-dependent antibody production by driving the expansion rather than the differentiation or extrafollicular migration of early plasmablasts. *J. Immunol.* 183:3139–3149. http://dx.doi.org/10.4049/jimmunol.0901690

Chan, T.D., K. Wood, J.R. Hermes, D. Butt, C.J. Jolly, A. Basten, and R. Brink. 2012. Elimination of germinal-center-derived self-reactive B cells is governed by the location and concentration of self-antigen. *Immunity.* 37:893–904. http://dx.doi.org/10.1016/j.immuni.2012.07.017

El Shikh, M.E., R.M. El Sayed, S. Sukumar, A.K. Szakal, and J.G. Tew. 2010. Activation of B cells by antigens on follicular dendritic cells. *Trends Immunol.* 31:205–211. http://dx.doi.org/10.1016/j.it.2010.03.002

Falini, B., M. Fizzotti, A. Pucciarini, B. Bigerna, T. Marafioti, M. Gambacorta, R. Pacini, C. Alunni, L. Natali-Tanci, B. Ugolini, et al. 2000. A monoclonal antibody (MUM1p) detects expression of the MUM1/IRF4 protein in a subset of germinal center B cells, plasma cells, and activated T cells. *Blood.* 95:2084–2092.

Gatto, D., and R. Brink. 2010. The germinal center reaction. *J. Allergy Clin. Immunol.* 126:898–907. http://dx.doi.org/10.1016/j.jaci.2010.09.007

Goodnow, C.C., C.G. Vinuesa, K.L. Randall, F. Mackay, and R. Brink. 2010. Control systems and decision making for antibody production. *Nat. Immunol.* 11:681–688. http://dx.doi.org/10.1038/ni.1900

Hodgkin, P.D., B.E. Castle, and M.R. Kehry. 1994. B cell differentiation induced by helper T cell membranes: evidence for sequential isotype switching and a requirement for lymphokines during proliferation. *Eur. J. Immunol.* 24:239–246. http://dx.doi.org/10.1002/eji.1830240138

Horikawa, K., S.W. Martin, S.L. Pogue, K. Silver, K. Peng, K. Takatsu, and C.C. Goodnow. 2007. Enhancement and suppression of signaling by the conserved tail of IgG memory-type B cell antigen receptors. *J. Exp. Med.* 204:759–769. http://dx.doi.org/10.1084/jem.20061923

Jacob, J., G. Kelsoe, K. Rajewsky, and U. Weiss. 1991. Intraclonal generation of antibody mutants in germinal centres. *Nature.* 354:389–392. http://dx.doi.org/10.1038/354389a0

Jensen, G.S., S. Poppema, M.J. Mant, and L.M. Pilarski. 1989. Transition in CD45 isoform expression during differentiation of normal and abnormal B cells. *Int. Immunol.* 1:229–236. http://dx.doi.org/10.1093/intimm/1.3.229

Kallies, A., J. Hasbold, D.M. Tarlinton, W. Dietrich, L.M. Corcoran, P.D. Hodgkin, and S.L. Nutt. 2004. Plasma cell ontogeny defined by quantitative changes in blimp-1 expression. *J. Exp. Med.* 200:967–977. http://dx.doi.org/10.1084/jem.20040973

Khalil, A.M., J.C. Cambier, and M.J. Shlomchik. 2012. B cell receptor signal transduction in the GC is short-circuited by high phosphatase activity. *Science.* 336:1178–1181. http://dx.doi.org/10.1126/science.1213368

Lalor, P.A., G.J. Nossal, R.D. Sanderson, and M.G. McHeyzer-Williams. 1992. Functional and molecular characterization of single, (4-hydroxy-3-nitrophenyl)acetyl (NP)-specific, $IgG_1^+$ B cells from antibody-secreting and memory B cell pathways in the C57BL/6 immune response to NP. *Eur. J. Immunol.* 22:3001–3011. http://dx.doi.org/10.1002/eji.1830221136

Meyer-Hermann, M.E., P.K. Maini, and D. Iber. 2006. An analysis of B cell selection mechanisms in germinal centers. *Math. Med. Biol.* 23:255–277. http://dx.doi.org/10.1093/imammb/dql012

Meyer-Hermann, M., E. Mohr, N. Pelletier, Y. Zhang, G.D. Victora, and K.M. Toellner. 2012. A theory of germinal center B cell selection, division, and exit. *Cell Reports.* 2:162–174. http://dx.doi.org/10.1016/j.celrep.2012.05.010

Mori, S., R.E. Rempel, J.T. Chang, G. Yao, A.S. Lagoo, A. Potti, A. Bild, and J.R. Nevins. 2008. Utilization of pathway signatures to reveal distinct types of B lymphoma in the Emicro-myc model and human diffuse large B-cell lymphoma. *Cancer Res.* 68:8525–8534. http://dx.doi.org/10.1158/0008-5472.CAN-08-1329

Nowosad, C.R., K.M. Spillane, and P. Tolar. 2016. Germinal center B cells recognize antigen through a specialized immune synapse architecture. *Nat. Immunol.* 17:870–877. http://dx.doi.org/10.1038/ni.3458

Paus, D., T.G. Phan, T.D. Chan, S. Gardam, A. Basten, and R. Brink. 2006. Antigen recognition strength regulates the choice between extrafollicular plasma cell and germinal center B cell differentiation. *J. Exp. Med.* 203:1081–1091. http://dx.doi.org/10.1084/jem.20060087

Phan, T.G., M. Amesbury, S. Gardam, J. Crosbie, J. Hasbold, P.D. Hodgkin, A. Basten, and R. Brink. 2003. B cell receptor-independent stimuli trigger immunoglobulin (Ig) class switch recombination and production of IgG autoantibodies by anergic self-reactive B cells. *J. Exp. Med.* 197:845–860. http://dx.doi.org/10.1084/jem.20022144

Phan, T.G., D. Paus, T.D. Chan, M.L. Turner, S.L. Nutt, A. Basten, and R. Brink. 2006. High affinity germinal center B cells are actively selected into the plasma cell compartment. *J. Exp. Med.* 203:2419–2424. http://dx.doi.org/10.1084/jem.20061254

Plotkin, S.A., W.A. Orenstein, and P.A. Offit. 2008. Vaccines. Elsevier, Philadelphia. 1570 pp.

Sciammas, R., A.L. Shaffer, J.H. Schatz, H. Zhao, L.M. Staudt, and H. Singh. 2006. Graded expression of interferon regulatory factor-4 coordinates isotype switching with plasma cell differentiation. *Immunity.* 25:225–236. http://dx.doi.org/10.1016/j.immuni.2006.07.009

Shinnakasu, R., T. Inoue, K. Kometani, S. Moriyama, Y. Adachi, M. Nakayama, Y. Takahashi, H. Fukuyama, T. Okada, and T. Kurosaki. 2016. Regulated selection of germinal-center cells into the memory B cell compartment. *Nat. Immunol.* 17:861–869. http://dx.doi.org/10.1038/ni.3460

Smith, K.G., A. Light, L.A. O'Reilly, S.M. Ang, A. Strasser, and D. Tarlinton. 2000. *bcl-2* transgene expression inhibits apoptosis in the germinal center and reveals differences in the selection of memory B cells and bone marrow antibody-forming cells. *J. Exp. Med.* 191:475–484. http://dx.doi.org/10.1084/jem.191.3.475

Smith-Gill, S.J., T.B. Lavoie, and C.R. Mainhart. 1984. Antigenic regions defined by monoclonal antibodies correspond to structural domains of avian lysozyme. *J. Immunol.* 133:384–393.

Victora, G.D., and M.C. Nussenzweig. 2012. Germinal centers. *Annu. Rev. Immunol.* 30:429–457. http://dx.doi.org/10.1146/annurev-immunol-020711-075032

Victora, G.D., T.A. Schwickert, D.R. Fooksman, A.O. Kamphorst, M. Meyer-Hermann, M.L. Dustin, and M.C. Nussenzweig. 2010. Germinal center dynamics revealed by multiphoton microscopy with a photoactivatable fluorescent reporter. *Cell.* 143:592–605. http://dx.doi.org/10.1016/j.cell.2010.10.032